Journal of Power Sources 222 (2013) 448–454

Contents lists available at SciVerse ScienceDirect

Journal of Power Sources

journal homepage: www.elsevier.com/locate/jpowsour

Structural and thermodynamic stability of $Li_4Ti_5O_{12}$ anode material for lithium-ion battery

Ting-Feng Yi [a,c,*], Ying Xie [b,**], Yan-Rong Zhu [a], Rong-Sun Zhu [a], Haoyu Shen [c]

[a] School of Chemistry and Chemical Engineering, Anhui University of Technology, No.59 Hudong Road, Maanshan, Anhui 243002, PR China
[b] Key Laboratory of Functional Inorganic Material Chemistry, Ministry of Education, School of Chemistry and Materials Science, Heilongjiang University, Harbin 150080, PR China
[c] Chilwee Power Co., Ltd, Changxing, Zhejiang 313100, PR China

HIGHLIGHTS

- The relationship between the thermodynamic stability and microscopic bonding of $Li_4Ti_5O_{12}$ is investigated.
- The low formation enthalpy indicates that spinel $Li_4Ti_5O_{12}$ has a high thermodynamic stability.
- PF_5 is the main species which damages the SEI layer.

GRAPHICAL ABSTRACT

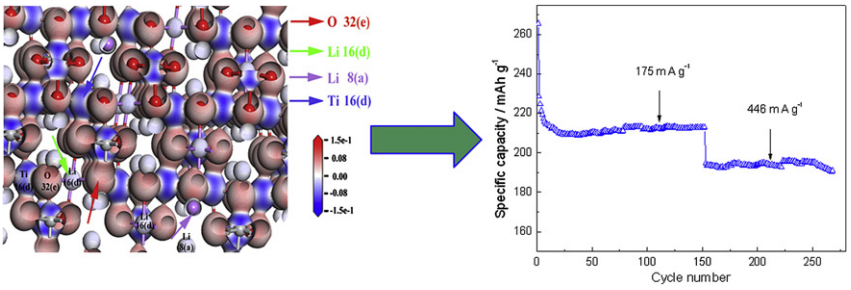

ARTICLE INFO

Article history:
Received 24 May 2012
Received in revised form
30 July 2012
Accepted 4 September 2012
Available online 14 September 2012

Keywords:
Thermodynamic stability
Density functional theory
Lithium-ion battery
Anode
Lithium titanate

ABSTRACT

The structural and thermal stability are essential to understand the safety of $Li_4Ti_5O_{12}$, but it is not fully understood. Here, the structural and thermal stability were investigated by the density functional theory (DFT) plane-wave pseudopotential technique and experimental method. Sub-micro $Li_4Ti_5O_{12}$ particles were synthesized by a solid-state reaction. The calculated results of lattice parameters are highly coincident with the experimental values. XRD and Raman spectra demonstrate the formation of pure phase $Li_4Ti_5O_{12}$. There is an amorphous phase and no phase transition when discharged to 0 V, which confirms that there is a certain reversible intercalation processes cycled below 1 V instead of a reduction–decomposition reaction. SEM shows that $Li_4Ti_5O_{12}$ powder has a uniform, nearly cubic structural morphology with a narrow size distribution of about 500 nm. The low formation enthalpy (-6061.45 ± 4) indicates that $Li_4Ti_5O_{12}$ has a high thermodynamic stability. The superior cycling performance at high rates cycled between 0 and 2.5 shows that $Li_4Ti_5O_{12}$ has a very high structural stability. The high thermodynamic stability of $Li_4Ti_5O_{12}$ is related to the strong covalent bonding characteristic between Ti and O according to the electron density difference diagram. DSC reveals that PF_5 is the main species which damages the SEI layer.

1. Introduction

The high energy density of lithium-ion battery has made it the battery of choice in applications ranging from cell phones and laptops to large hybrid electric vehicles (HEVs) and electric vehicles (EVs) [1,2]. EVs and HEVs are seen as the main answer to the transport sector's problems of diminishing oil supplies and global warming. The safety issue acquires particular importance in the

* Corresponding author. School of Chemistry and Chemical Engineering, Anhui University of Technology, No.59 Hudong Road, Maanshan, Anhui 243002, PR China. Tel.: +86 555 2311807; fax: +86 555 2311552.
** Corresponding author.
E-mail addresses: tfyihit@163.com (T.-F. Yi), xieying@hlju.edu.cn (Y. Xie).

0378-7753/$ – see front matter © 2012 Elsevier B.V. All rights reserved.
http://dx.doi.org/10.1016/j.jpowsour.2012.09.020

case of batteries for EVs and HEVs. Graphite is the most commonly used anode material in lithium-ion batteries. At full charge, the highly lithiated graphite (LiC_6) electrode is highly reactive because it operates close to the potential of metallic lithium, keeping to a large extent the safety issue. Propylene carbonate (PC)-based electrolytes presents interesting properties since it is able to dissolve and dissociate lithium salts leading to highly conducting electrolytes even at low temperatures. Moreover, electrolytes containing PC as a unique solvent are stable against oxidation to about 5 V [3] .On the other hand, PC-based electrolyte is preferred in lithium-ion batteries due to the enhanced safety characteristics and ability to operate the batteries at low temperatures. Unfortunately, during the reduction of graphite, PC is decomposed at a lower potential lower rather than that corresponding to the intercalation of solvated lithium ions, and the irreversible reactions can cause severe exfoliation to the graphite structure [4–6]. In addition, the main drawback for carbonaceous materials is the solid electrolyte interface (SEI) passivation film formed during the first charge process can decompose at higher temperature, and then induce failure of the cell and even ignition of the battery [7]. Safety is mainly related to the thermal reactivity of electrode material. Hence, it can be concluded that the thermal stability of negative electrode is a critical factor for the safety of lithium-ion batteries. In order to address the safety limitations of lithium-ion cells, spinel lithium titanate ($Li_4Ti_5O_{12}$) has been proposed as an alternative to carbon anode in lithium-ion batteries due to the inherent safety and compatibility with the electrolyte [8–11]. Several authors reported that the reaction of $Li_4Ti_5O_{12}$ with lithium ion shows one typical reversible insertion/extraction process cycled between 1.0 and 2.0 V when the amount of inserted lithium ions are limited within three [12,13]. Our group and other authors have reported that SEI film of $Li_4Ti_5O_{12}$ was formed at below 0.7 V in the first discharge process, but it is an SEI film free material when it was cycled above 1.0 V [14–16]. Hence, the structural and thermal stability (down to 0 V) is important to the safety of $Li_4Ti_5O_{12}$. In addition, experimental research on $Li_4Ti_5O_{12}$ only provides experimental data and little theoretical studies have been done, so it is necessary to study the basic structural and thermal stability properties from both the theoretical and experimental point of view. Ouyang et al. [17] investigated the structural and electronic properties of $Li_4Ti_5O_{12}$ spinel by density functional theory (DFT) calculations. Zhong et al. [18] reported that $Li_4Ti_5O_{12}$ can be lithiated to the state $Li_{8.5}Ti_5O_{12}$, which provides a theoretical capacity that is about 1.5 times higher than that of the compound lithiated to $Li_7Ti_5O_{12}$ by means of first-principles calculations. Liu et al. [19] investigated the electronic band structures of pristine and Cr-, Fe-, Ni- or Mg-doped $Li_4Ti_5O_{12}$ calculated by the first-principles local density calculations. To our knowledge, the structural and thermal stability (down to 0 V) of $Li_4Ti_5O_{12}$ are not reported. With this consideration, spinel $Li_4Ti_5O_{12}$ was synthesized by a solid-state method, and the relationship between the thermodynamic stability and microscopic bonding of the compounds were investigated on the basis of first-principles predictions.

2. Experimental and theoretical calculations

2.1. Materials preparation

$Li_4Ti_5O_{12}$ samples were prepared using a solid-state method from the mixture of TiO_2-anatase (AR) and Li_2CO_3 (AR) in a Li:Ti molar ratio of 4.3:5. Excess Li was provided to compensate for lithium volatilization during the high temperature synthesis. The precursors were ball-milled for 8 h and calcined at 850 °C for 24 h in air, then cooled down to room temperature.

2.2. Materials characterization

X-ray diffractometry (XRD) measurements were performed on a Rigaku instrument with Cu Kα radiation ($10^\circ < 2\theta < 90^\circ$). Scanning electron microscopy (SEM, Hitachi instrument) was performed to observe the particles morphology. The Raman spectra were recorded at room temperature with a Renishaw inVia 1000 micro-Raman system using a 514.2 nm excitation line from an Ar^+-ion laser (300 mW). Charge–discharge performance was characterized galvanostatically on Land 2000T (China) tester at different charge–discharge rates between 0 and 2.5 V (versus Li/Li^+). Cyclic voltammograms (CV) of $Li_4Ti_5O_{12}$/Li cell is measured on an electrochemical workstation (CHI 852C, China) between 0 and 3 V (versus Li/Li^+) at a scanning rate of 0.2 mV s^{-1}. Differential scanning calorimetric (DSC) measurements were conducted on NETZSCH STA 449C differential scanning calorimeter at a scanning rate of 5 °C min^{-1} from 30 to 300 °C in an Ar atmosphere. Sample for thermal analysis was sealed in an aluminum crucible. Electrode after cycles was taken out from batteries, and put into the aluminum crucible, then pressed to seal. All samples for thermal analysis were constructed in an Ar-filled glove box.

2.3. Preparation of lithium-ion batteries

The electrodes were prepared by mixing 80 wt.% active materials with 10 wt.% carbon black (CB) and 10 wt.% polyvinylidene fluoride (PVDF) dissolved in N-methyl-2-pyrrolidone (NMP) onto a Cu foil. The slurry was uniformly spread on Cu foil by a doctor blade technique. After coating, the film was dried in a vacuum oven at 120 °C for 12 h. Before use, the sheets were dried in a vacuum chamber at 120 °C for 10 h to avoid possible contamination with water. The coin cells were fabricated with the $Li_4Ti_5O_{12}$, metallic lithium anode, 1 M $LiPF_6$ in 1:1 ethylene carbonate (EC) and dimethyl carbonate (DMC) electrolyte, and Celgard polypropylene separator. The moisture contents are less than 10 ppm.

2.4. Theory and computation details

The present calculations were performed in the DFT framework [20] implemented in the CASTEP package [21]. In order to satisfy the stoichiometry of $Li_4Ti_5O_{12}$, a primitive cell with two $LiTi_2O_4$ units shown in Fig. 1a was constructed at first. To achieve the stoichiometry of Li4Ti5O12, a $1 \times 1 \times 3$ supercell was modeled. Two 16(d) site titanium atoms were substituted by lithium ones. The schemes of lithium-ion intercalation process for $Li_4Ti_5O_{12}$ are plotted in Fig. 1b–d. It is hard to find reliable and generally applicable expressions for the exchange correlation functionals, while the contributions of exchange correlation energy to the total energy are rather important and can be different to a large extent. Therefore, it is very necessary to determine the equilibrium configuration through series tests with different exchange correlation functionals. The generalized gradient approximation (GGA) potentials proposed by Perdew et al. (GGA-PBE) [22], Wu and Cohen (GGA-WC) [23], Perdew and Wang (PW91) [24], and Perdew et al. (GGA-RPBE) [25] as well as the local density approximation (LDA) potential by Ceperley–Alder and Perdew–Zunger (CA–PZ) [26,27] were considered during the tests. The electronic wave functions were expanded in terms of a plane-wave (PW) basis set, and the used energy cut off is 450 eV. The integration over the supercell irreducible Brillouin zone was treated by a $5 \times 5 \times 3$ mesh generated by the Monkhorst–Pack scheme. The total energy convergence is within 5.0×10^{-6} eV $atom^{-1}$.

3. Results and discussion

In order to find if there is structure stability, crystallographic characterization of $Li_4Ti_5O_{12}$ discharged to 0 V was carried out.

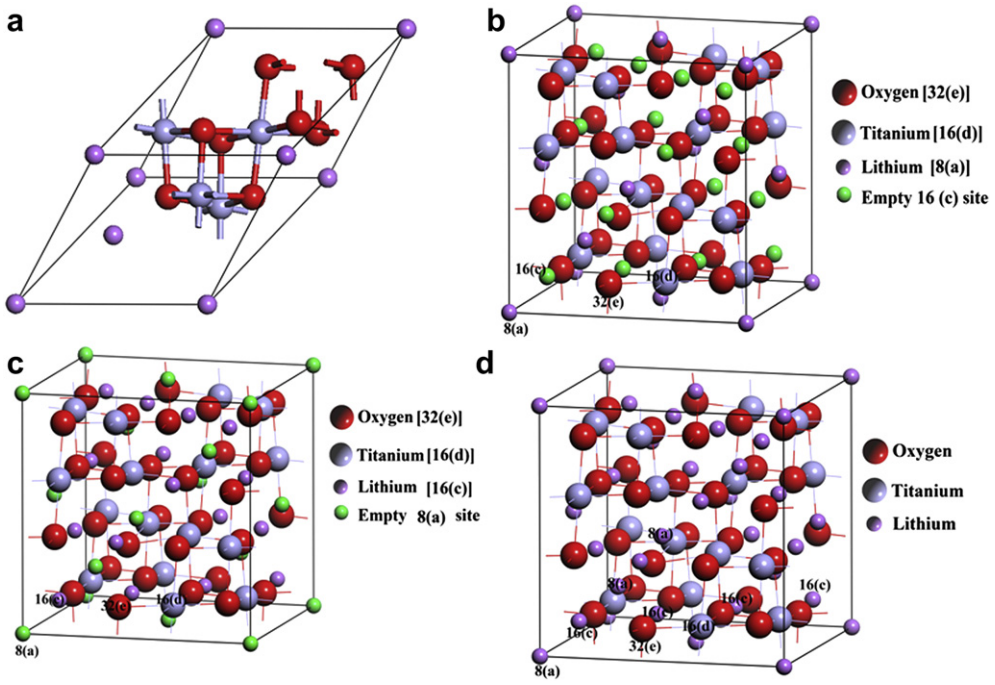

Fig. 1. $LiTi_2O_4$ crystal and scheme for lithium-ion intercalation process of $Li_{4+x}Ti_5O_{12}$ ($0 \le x \le 5$). (a) Primitive cell ($2LiTi_2O_4$ units). In the $Li_4Ti_5O_{12}$, oxygen and lithium occupy 32(e) and 8(a) sites, respectively, while 16(d) sites are occupied by titanium and lithium with a ratio of 5:1. The environment for 8a and 8b sites is equivalent. According to the different configurations, $Li_{4+x}Ti_5O_{12}$ ($0 \le x \le 5$) can be further denoted as: (b) $Li_4Ti_5O_{12}$: $[Li_3]_{8a}[\ ]_{16c}[Ti_5Li]_{16d}[O_{12}]_{32e}$; (c) $Li_7Ti_5O_{12}$: $[\ ]_{8a}[Li_6]_{16c}[Ti_5Li]_{16d}[O_{12}]_{32e}$; (d) $Li_9Ti_5O_{12}$: $[Li_x]_{8a}[Li_y]_{8b}[Li_6]_{16c}[Li_{2-x-y}]_{48f}\ [Ti_5Li]_{16d}[O_{12}]_{32e}$.

Fig. 2 shows the XRD patterns of $Li_4Ti_5O_{12}$ powder and $Li_4Ti_5O_{12}$ discharged to 0 V.

From Fig. 2a it can be observed that the patterns for $Li_4Ti_5O_{12}$ represent a single-phase cubic material with an Fd-3m space group. Compared with the Fig. 2a, some extra peaks such as copper (current collector) and PVDF (binder) are also detected as plotted in Fig. 2b. It is found that there is an amorphous phase when discharged to 0 V. This indicates that it is a certain reversible intercalation processes cycled below 1 V instead of a reduction–decomposition reaction, and then proves that $Li_4Ti_5O_{12}$ material has high structure stability during over discharge. According to the first principle calculation [18], $Li_7Ti_5O_{12}$ can not be transferred into $Li_9Ti_5O_{12}$ (should be $Li_{8.5}Ti_5O_{12}$) when discharged to 0 V. The further insertion of lithium into $Li_{8.5}Ti_5O_{12}$ is not allowed because

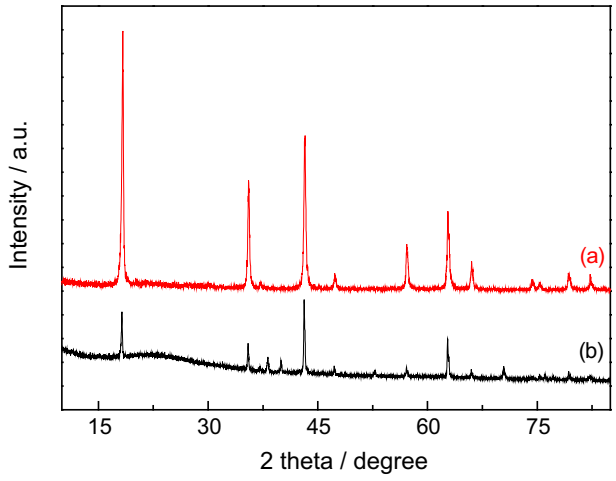

Fig. 2. X-ray diffraction patterns for (a) $Li_4Ti_5O_{12}$ powders; (b): $Li_4Ti_5O_{12}$ discharged to 0 V ($Li_{8.5}Ti_5O_{12}$).

the predicted intercalation potential becomes negative. Hence, it can be concluded that the valence of the Ti discharged to 0 V should be +3 and +4. According to the charge balance, the ratio between Ti^{3+} and Ti^{4+} is about 9:1. In addition, the intensity ratio in diffractograms of $Li_4Ti_5O_{12}$ and $Li_{8.5}Ti_5O_{12}$ is different. The reason may be that $Li_4Ti_5O_{12}$ is spinel structure, but $Li_{8.5}Ti_5O_{12}$ may be amorphous phase.

Fig. 3 shows Raman spectra (RS) and SEM image of $Li_4Ti_5O_{12}$ powder. The RS features are in good agreement with the feature of the spinel structure (A1g + Eg + 3F2g) [28–31]. This observation demonstrates the formation of phase-pure $Li_4Ti_5O_{12}$ [31]. This comment is well consistent with the XRD results mentioned above. $Li_4Ti_5O_{12}$ powder has a uniform, nearly cubic structural morphology with narrow size distribution about 500 nm.

In order to ensure the accuracy of the calculation, some tests based on $LiTi_2O_4$ were performed and the results are given in Table 1. The error (E) can be described by the equations,

$$E = \left| \frac{a_c - a_e}{a_e} \times 100\% \right| \quad (1)$$

where a_c and a_e are the calculated and experimental values of lattice parameters, respectively.

As we know, $Li_4Ti_5O_{12}$ is derived from $3(LiTi_2O_4)$ when one-sixth of the 16(d) site titaniums were substituted by lithiums. Therefore, it can be expected that the lattice parameters between $Li_4Ti_5O_{12}$ and $LiTi_2O_4$ should be very close. According to the experiments, the lattice parameters of $Li_4Ti_5O_{12}$ calculated through the least square program method from the diffraction data of Fig. 2 is 8.371 Å. The value is indeed very close to the 8.405 Å of $LiTi_2O_4$ [32]. From Table 1, it can be seen that the calculated results are highly coincident with the experimental results, and the biggest error is only 1.74% calculated by LDA CA–PZ. The smallest error is only 0.23% calculated by GGA-WC. Hence, The GGA-WC was used for the calculation of the electron exchange correlations energy.

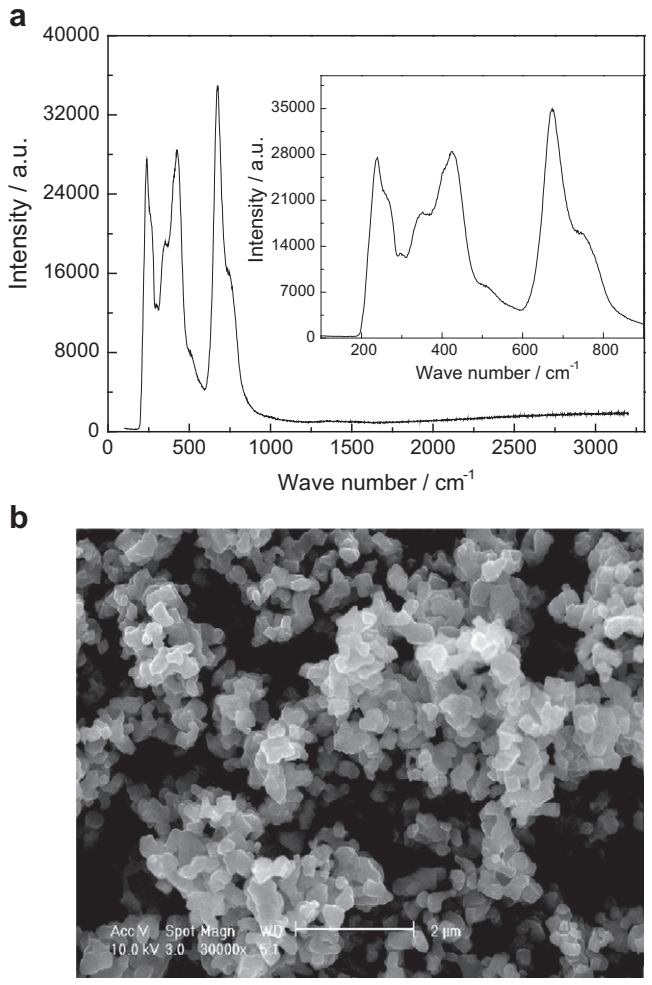

Fig. 3. (a) Raman spectra of $Li_4Ti_5O_{12}$ powder; (b) SEM image of as-synthesized $Li_4Ti_5O_{12}$ powder.

Despite some experiments [33–35] have proved the negligible structure variation of $Li_4Ti_5O_{12}$ during lithium insertion/extraction, it seems that no proper thermodynamic explanation has been given so far. It is therefore highly desired to examine the major factors of determining the structure stability by calculating molar formation enthalpy (Δ_fH_m) of $Li_4Ti_5O_{12}$ and to make it possible to adopt a material-design approach. To obtain the formation enthalpy, the molar reaction enthalpy (Δ_rH_m) is derived from the crystal energies first. Relying on the thermodynamic cycle described below

$$2Li_2O\ (s) + 5TiO_2\ (s) \rightarrow Li_4Ti_5O_{12}\ (s) \quad (2)$$

Δ_rH_m can be calculated by,

$$\begin{aligned}\Delta_rH_m &= \Delta_fH_m(Li_4Ti_5O_{12}) - 2\Delta_fH_m(Li_2O) \\ &\quad - 5\Delta_fH_m(TiO_2(\text{rutile})) \\ &= E(Li_4Ti_5O_{12}) - 2E(Li_2O) - 5E(TiO_2(\text{rutile}))\end{aligned} \quad (3)$$

Table 1
Calculated and experimental lattice parameters of $LiTi_2O_4$.

Function	LDA CA–PZ	GGA-PW91	GGA-PBE	GGA-RPBE	GGA-WC	Experiment [32]
Lattice parameters (Å)	8.259	8.457	8.457	8.528	8.386	8.405
Error (%)	1.74	0.619	0.619	1.46	0.226	–

where $E(Li_2O)$, $E(TiO_2)$ (s, rutile), and $E(Li_4T_5O_{12})$ represent the total energies of Li_2O (−821.0508701 ev), TiO_2 (−2483.333688 eV), and $Li_4Ti_5O_{12}$ crystals (−14060.26244 eV), respectively. Because the entropy change and volume effect of solid material can be neglected [36], the molar reaction enthalpy (Δ_rH_m) can be determined by the DFT total energies and is calculated to be −143.99 kJ mol^{-1}. According to the thermodynamic data for substances, the Δ_fH_m values for TiO_2 (s, rutile) and Li_2O are −944.0 ± 0.8 and −598.730 kJ mol^{-1} respectively [37]. On the basis of the following equation,

$$\begin{aligned}\Delta_fH_m(Li_4Ti_5O_{12}) &= \Delta_rH_m + 2\Delta_fH_m(Li_2O) \\ &\quad + 5\Delta_fH_m(TiO_2,\ s,\ \text{rutile})\end{aligned} \quad (4)$$

The formation enthalpy (Δ_fH_m) of $Li_4T_5O_{12}$ is finally determined to be −6061.45 ± 4 kJ mol^{-1}. The calculated formation enthalpies of $Li_4Ti_5O_{12}$ can be compared with the estimated value (−6170.06 kJ mol^{-1}) using two-parameter model and congeneric linear rule [38]. The low formation enthalpy ($1/3\Delta_fH_m = -2020.48 \pm 1.333$ kJ mol^{-1}) indicates that spinel $Li_{4/3}Ti_{5/3}O_4$ ($1/3[Li_4Ti_5O_{12}]$) has a high structural stability, and higher than that of spinel $LiMn_2O_4$ (−1229.48 kJ mol^{-1}) and $LiMn_{1.5}Ni_{0.5}O_4$ (−1351.34 kJ mol^{-1}) from our previous work [39].

The thermodynamic cycle of $Li_7Ti_5O_{12}$ and $Li_{8.5}Ti_5O_{12}$ described below

$$2Li_2O\ (s) + 5TiO_2\ (s) + 3Li\ (s) \rightarrow Li_7Ti_5O_{12}\ (s) \quad (5)$$

$$2Li_2O\ (s) + 5TiO_2\ (s) + 4.5Li\ (s) \rightarrow Li_{8.5}Ti_5O_{12}\ (s) \quad (6)$$

where $E(Li_2O)$, $E(Li)$, $E(TiO_2)$ (s, rutile), and $E(Li_7Ti_5O_{12})$ represent the total energies of Li_2O, Li (−190.19579 eV), TiO_2, $Li_7Ti_5O_{12}$ (−14636.002 eV), and $Li_{8.5}Ti_5O_{12}$ crystals (−14920.593 eV), respectively. Hence, the molar reaction enthalpy (Δ_rH_m) of $Li_7Ti_5O_{12}$ and $Li_{8.5}T_5O_{12}$ can be calculated to be −641.12 and −573.32 kJ mol^{-1}, respectively. The molar formation enthalpy (Δ_fH_m) of $Li_7Ti_5O_{12}$ and $Li_{8.5}Ti_5O_{12}$ can be calculated according to the following equations:

$$\begin{aligned}\Delta_fH_m(Li_7Ti_5O_{12}) &= \Delta_rH_m + 2\Delta_fH_m(Li_2O) \\ &\quad + 5\Delta_fH_m(TiO_2,\ s,\ \text{rutile}) + 3\Delta_fH_m(Li)\end{aligned} \quad (7)$$

$$\begin{aligned}\Delta_fH_m(Li_{8.5}Ti_5O_{12}) &= \Delta_rH_m + 2\Delta_fH_m(Li_2O) \\ &\quad + 5\Delta_fH_m(TiO_2,\ s,\ \text{rutile}) + 4.5\Delta_fH_m(Li)\end{aligned} \quad (8)$$

The formation enthalpy (Δ_fH_m) of $Li_7Ti_5O_{12}$ and $Li_{8.5}Ti_5O_{12}$ is finally determined to be −6558.58.45 ± 4 and −6490.78 ± 4 kJ mol^{-1}, respectively. The difference of molar formation enthalpy between $Li_7Ti_5O_{12}$ and $Li_{8.5}Ti_5O_{12}$ is very little. According to the calculated values, the thermodynamic stability of $Li_4T_5O_{12}$ can be further improved after the Li^+ intercalation of $Li_7Ti_5O_{12}$, but the thermodynamic stability can be diminished after the Li^+ intercalation of $Li_{8.5}Ti_5O_{12}$. Hence, it can be concluded that both $Li_7T_5O_{12}$ and $Li_{8.5}T_5O_{12}$ also have high thermodynamic stability.

Galvanostatic charge–discharge profile and rate capability curves between 0 and 2 V are shown in Fig. 4. It can be seen that all materials show a loss of the 1.55 V plateau with increasing the cycling number. It is obvious that additional 20–30% capacity comes from lithium storage below 1.0 V. It can be found that there is an irreversible capacity loss when the cutoff voltage for discharging is limited to 0.0 V. The reason has been explained in our

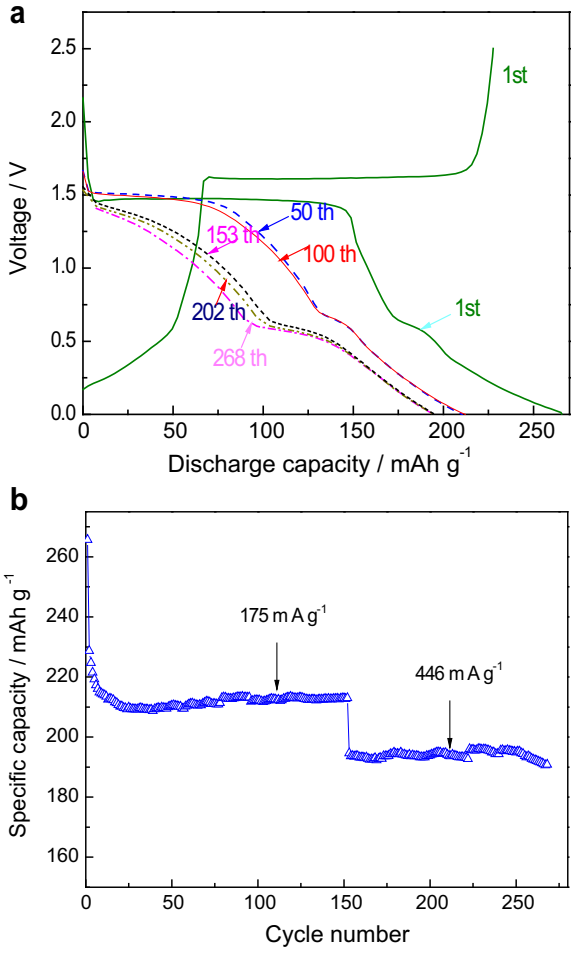

Fig. 4. (a) Charge and discharge curves of $Li_4Ti_5O_{12}$ obtained from a CR 2032 coin-type half cell using Li metal as the anode (1–152 cycles corresponds to 175 mA g^{-1} and 153–268 cycles corresponds to 446 mA g^{-1}) and (b) rate capability of $Li_4Ti_5O_{12}$. Same charge and discharge C-rate.

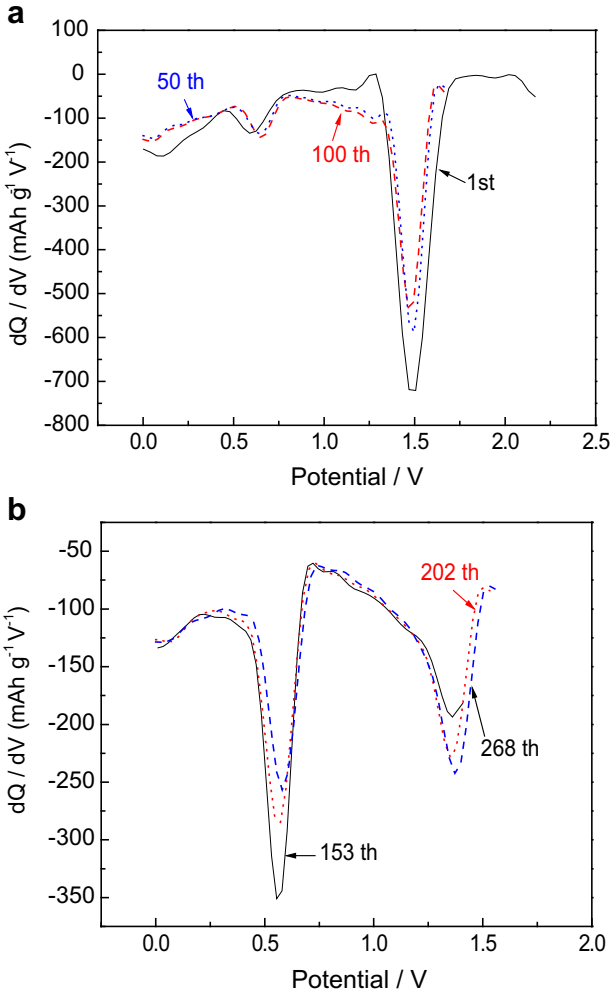

Fig. 5. Differential capacity vs voltage plots of $Li_4Ti_5O_{12}$ obtained from Fig. 4 charge–discharged at (a) 175 mA g^{-1} and (b) 446 mA g^{-1}.

previous work [14,31]. It is easy to understand all the electrochemical energy comes from reversible redox reactions between trivalent titanium ion (Ti^{3+}) and tetravalent titanium ion (Ti^{4+}). According to the different configurations as plotted in Fig. 1, $Li_{4+x}Ti_5O_{12}$ ($0 \le x \le 5$) can be further denoted as $[Li_3]_{8a}[\ ]_{16c}[Ti_5Li]_{16d}[O_{12}]_{32e}$ ($Li_4Ti_5O_{12}$), $[\ ]_{8a}[Li_6]_{16c}[Ti_5Li]_{16d}[O_{12}]_{32e}$ ($Li_7Ti_5O_{12}$) corresponding to the 1.55 V plateau and $[Li_x]_{8a}[Li_y]_{8b}[Li_6]_{16c}[Li_{2-x-y}]_{48f}[Ti_5Li]_{16d}[O_{12}]_{32e}$ ($Li_9Ti_5O_{12}$) corresponding to the capacity below 1.0 V. As confirmed in the rate capability data (Fig. 4b), the obtained capacities are above 195 mA h g^{-1} throughout cycling even though the applied current was increased to the 446 mA g^{-1}. The superior cycling performance at high charge–discharged rates cycled between 0 and 2.5 shows that $Li_4Ti_5O_{12}$ has a very high structural stability. This can be compared with the calculated formation enthalpy of $Li_4Ti_5O_{12}$ mentioned above. The differential capacity discharge curves between 0 and 2.5 V from Fig. 4 are shown in Fig. 5.

It can be seen that the material shows a loss of the 1.55 V plateau with increasing the cycling number and the 0.7 V plateau obviously increases with increasing the discharge rate. These results indicate that the electrochemical lithium extraction/insertion reaction in these composite anode materials takes place in at least two stages during cycling. A plateau is at around 1.55 V, which is in good agreement with the two-phase reaction between spinel structure of $Li_4Ti_5O_{12}$ and rock-salt structure of $Li_7Ti_5O_{12}$ [31,40]. The plateau at about 0.5 V may correspond to a single-phase transition of rock-salt from $Li_7Ti_5O_{12}$ to $Li_{8.5}Ti_5O_{12}$ [41]. At a high current rate discharge, the two-phase conversion from $Li_4Ti_5O_{12}$ to $Li_7Ti_5O_{12}$ cannot be completely carried out in a limited time due to the intrinsically poor conductivity. Hence, the 1.55 V plateau decreases due to the high current density during discharge. However, the single-phase transition of rock-salt from $Li_7Ti_5O_{12}$ to $Li_{8.5}Ti_5O_{12}$ may be easily carried out in a limited time. So, the 0.5 V plateau obviously increases at high current rate discharge. The discharge peaks of $Li_4Ti_5O_{12}$ at the 1st, 50th and 100th charge-discharged at 175 mA g^{-1} are about 1.506, 1.492 and 1.497 V, respectively. The discharge peaks at the 153th, 202th and 268th charge–discharged at 446 mA g^{-1} are about 1.363, 1.351 and 1.372 V, respectively. This can be concluded that $Li_4Ti_5O_{12}$ material has a little polarization and high structure stability during charge and discharge even at high rates.

The cyclic voltammetry of fresh $Li_4Ti_5O_{12}$/Li cell was performed as shown in Fig. 6. The figure clearly demonstrates that there are two pairs of redox peaks for each sample in the voltage range of 1.5–2.0 V associated with the reversible change of Ti^{4+} to Ti^{3+} and below 0.6 V due to another change of Ti^{4+} to Ti^{3+}. These results indicate that the electrochemical lithium extraction/insertion reaction in these composite electrode materials takes place in at least two stages during cycling. In addition, there is a broad peak with envelope feature at lower potentials, indicating a formation of amorphous phase during discharge to 0 V.

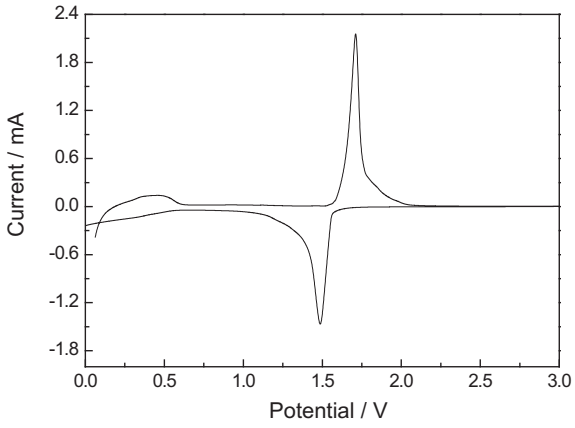

Fig. 6. Cyclic voltammerty (CV) for $Li_4Ti_5O_{12}$/Li cell between 0 and 3 V.

To further reveal the origin of stability from the microscopic point of view, we calculated the electron density differences of $Li_4Ti_5O_{12}$ as shown in Fig. 7. Due to the formation of covalent bonds, the electron distribution is changed. The positive (in red) or negative (in blue) (In the web version) regions indicate respectively where the electron density is enriched or depleted. From Fig. 7, it can be identified that covalent bonds between Ti and O atoms are formed, leading to some electron transformation from Ti to O atoms. It should be emphasized that in the compounds two kinds of lithium ions should be considered. The first kind is the 16(d) site lithium ions, and the second is the ordinary Li^+ at other positions. The results clear indicated that all the lithium exists in the crystal lattice as pure ions. Moreover, according to the electron redistribution characteristics, it can be further confirmed that O atoms take sp^3 hybridizations, and the hybrid orbits overlap effectively with the 3d ones of three nearest neighbor Ti atoms. Such covalent bonds formed between Ti-3d and O-2p orbits are of particularly importance to excellent thermodynamical stability of the compounds, since the stronger the covalent bonds, the more energy will be released due to the formation of bonds. In comparison to the pure $LiTi_2O_4$ compound (-2070.723 ± 1.6 kJ mol^{-1}) [42], the substitution of 16(d) site titanium by lithium results in a larger formation enthalpy ($\Delta_f H_m$ ($Li_{4/3}Ti_{5/3}O_4$) = -2020.48 ± 1.33 kJ mol^{-1}), which suggested that the stability of system is weakened due to the replacement.

DSC curves of $Li_4Ti_5O_{12}$ discharged to 1 and 0 V is shown in Fig. 8. There is two main exothermic peaks appear in the temperature range 50–280 °C. It has been reported that these thermal reactions may correspond to SEI layer breakdown, lithium–solute reaction, new surface layer probable breakdown and Li_2CO_3 formation process [43–48]. It has been reported that $LiPF_6$ is an unstable solute and can partly decompose into PF_5 and LiF in the electrolyte, and HF generated during cycling when using $LiPF_6$-based electrolyte. According to the literatures, it can be concluded that the signal observed at 111 °C is attributed to the reaction of dissociative PF_5 with available lithium from lithiated $Li_7Ti_5O_{12}$ ($Li_4Ti_5O_{12}$ discharged to 1 V).

The reaction mechanism is as follows [49–51]:

$$LiPF_6 \rightarrow LiF + PF_5 \quad (9)$$

$$PF_5 + H_2O \rightarrow 2HF + PF_3O \quad (10)$$

$$PF_5 + 2xe + 2xLi^+ \rightarrow xLiF + Li_xPF_{5-x} \quad (11)$$

$$PF_3O + 2xe + 2xLi^+ \rightarrow xLiF + Li_xPF_{3-x}O \quad (12)$$

$$PF_6^- + 2e + 3Li^+ \rightarrow 3LiF + PF_3 \quad (13)$$

Hence, LiF and other products may be the components of the new surface film, and formed by the reaction on the surface of the electrode particles [52]. If the water in the electrolyte is not considered, it can be suggested that PF_5 is the main species which damages the SEI layer based on physical and chemical characteristics of PF_5. Moreover, the destruction of SEI layer accelerates the

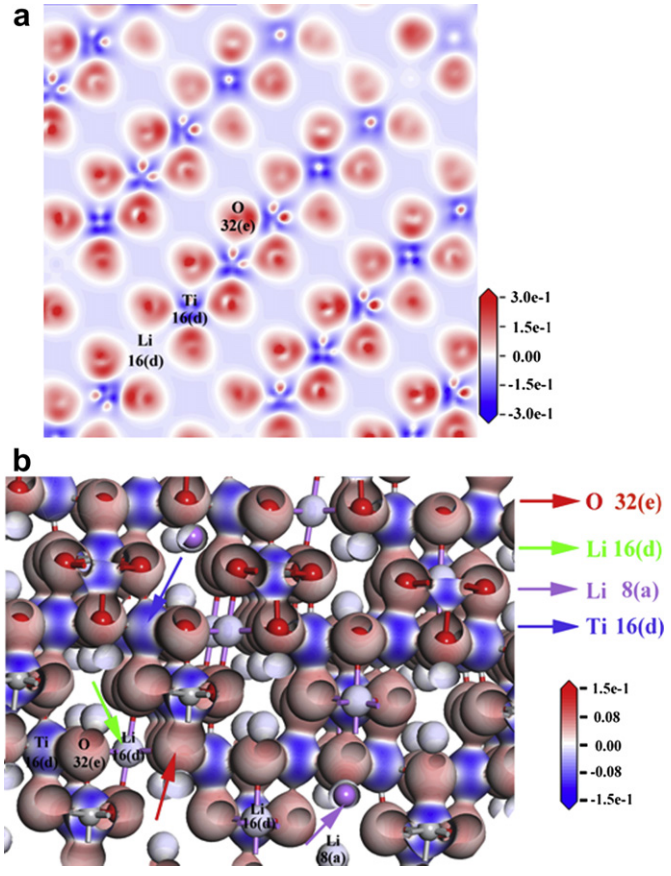

Fig. 7. Electron density difference diagram for $Li_4Ti_5O_{12}$ compounds: (a) view for (001) crystal plane and (b) three-dimensional view.

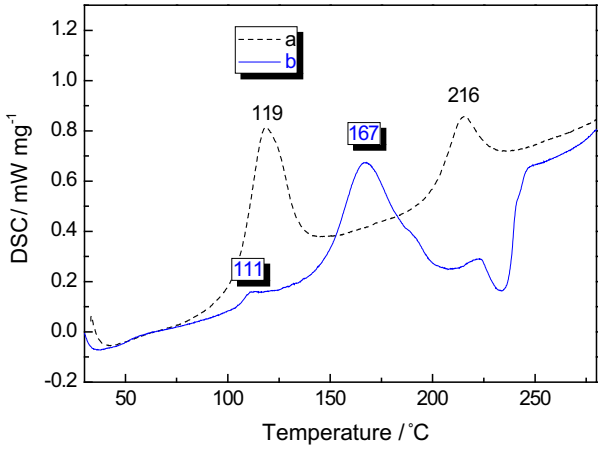

Fig. 8. DSC curves of $Li_4Ti_5O_{12}$ with different contents of intercalated lithium (a) $Li_{8.5}Ti_5O_{12}$ ($Li_4Ti_5O_{12}$ discharged to 0 V) and (b) $Li_7Ti_5O_{12}$ ($Li_4Ti_5O_{12}$ discharged to 1 V).

PF_5 and solvents to reach the lithiated compound surface. Hence, the existence of PF_5 may be the major source for the first exothermic process. The peak at 167 °C of $Li_7Ti_5O_{12}$ may correspond to the reaction of the intercalated lithium with the solvents. According to the composition of the electrolyte (EC and DMC), the intercalated lithium reacts with the solvents to produce lithium alkyl carbonate and then Li_2CO_3. The reaction mechanism is as follows.

One electron reaction to form lithium carbonate

$$EC + e \rightarrow EC^- \text{ free radical} \quad (14)$$

$$2EC^- \text{ free radical} + 2Li^+ \rightarrow C_2H_4 + \text{lithium alkyl carbonate} \quad (15)$$

Two-electron reaction to form lithium carbonate

$$EC + 2e \rightarrow C_2H_4 + CO_3^{2-} \quad (16)$$

$$CO_3^{2-} + 2Li^+ \rightarrow Li_2CO_3 \quad (17)$$

The thermal reaction of PVDF binder can be ignored because PVDF binder has a minimal effect on the thermal response of the anode reaction reported by Roth et al. [48]. The similar thermal reactions between available lithium and electrolyte (solute, solvent) of $Li_{8.5}Ti_5O_{12}$ ($Li_4Ti_5O_{12}$ discharged to 0 V) taken place near 119 and 216 °C.

It can be concluded that there is an earlier thermal reaction of $Li_7Ti_5O_{12}$ than that of $Li_{8.5}Ti_5O_{12}$. However, the exothermic peak area of the $Li_{8.5}Ti_5O_{12}$ sample is rather larger than the $Li_7Ti_5O_{12}$ sample. Hence, heat generation from the $Li_7Ti_5O_{12}$ is milder than that of the $Li_{8.5}Ti_5O_{12}$. Once the thermal reaction occurs, $Li_7Ti_5O_{12}$ has a higher thermal stability than that of the $Li_{8.5}Ti_5O_{12}$. The experimental result is well consistent with the calculated result mentioned above.

4. Conclusions

In this study, sub-micro $Li_4Ti_5O_{12}$ particles with narrow size distribution about 500 nm are synthesized by a solid-state reaction. The structural, electrochemical performance and thermal stability are investigated by the DFT plane-wave pseudopotential technology and experimental method. The equilibrium configuration is determined by the different exchange correlation functionals and pseudopotentials. There is an amorphous phase when $Li_4Ti_5O_{12}$ discharge to 0 V. RS features are in good agreement with the feature of the phase-pure spinel structure (A1g + Eg + 3F2g). The low formation enthalpy (-6061.45 ± 4 kJ mol^{-1}) calculated by GGA- WC indicates that spinel $Li_4Ti_5O_{12}$ has a high thermodynamic stability. The superior cycling performance can be concluded that $Li_4Ti_5O_{12}$ material has a little polarization and high structure stability during charge and discharge even at high rates, and then proves that $Li_4Ti_5O_{12}$ material has high structure stability during over discharge. Ti-3d orbit and O-2p orbits have an effective overlap, and then forms a strong covalent bond. It is an important thermodynamically stable factor for $Li_4Ti_5O_{12}$. DSC reveals that PF_5 is the main species which damages the SEI layer. The high thermodynamically stable $Li_4Ti_5O_{12}$ materials are well suited for application in high power energy storage devices including high power lithium batteries and hybrid devices.

Acknowledgments

This work was financially supported by the National Natural Science Foundation of China (Grant Nos. 50902001 and 51274002), the Key project of Scientific Research Foundation sponsored by Education Department of Anhui Province, China (no. KJ2010A045), and the Program for Innovative Research Team in Anhui University of Technology (no. TD201202). This work is also supported by the Natural Science Foundation of Heilongjiang Province (no. B201003), and Educational Commission of Heilongjiang Province (no. 11551340).

References

[1] T.A. Stuart, W. Zhu, J. Power Sources 196 (2011) 458.
[2] T. Horiba, K. Hironaka, T. Matsumura, T. Kai, M. Koseki, Y. Muranaka, J. Power Sources 119–121 (2003) 893.
[3] M. Arakawa, J.-I. Yamaki, J. Power Sources 54 (1995) 250.
[4] G. Chung, S. Jun, K. Lee, M. Kim, J. Electrochem. Soc. 146 (1999) 1664.
[5] T. Osaka, T. Momma, T. Tajima, Y. Matsumoto, J. Electrochem. Soc. 142 (1995) 1057.
[6] M.-S. Wu, P.-C. Julia Chiang, J.-C. Lin, J.-T. Lee, Electrochim. Acta 49 (2004) 4379–4386.
[7] M. Egashira, S. Okada, J. Yamaki, J. Power Sources 124 (2003) 237.
[8] T.-F. Yi, L.-J. Jiang, J. Shu, C.-B. Yue, R.-S. Zhu, H.-B. Qiao, J. Phys. Chem. Solids 71 (2010) 1236–1242.
[9] T. Ohzuku, A. Ueda, N. Yamamoto, J. Electrochem. Soc. 142 (1995) 1431–1435.
[10] K. Dokko, J.-I. Sugaya, H. Munakata, K. Kanamura, Electrochim. Acta 51 (2005) 966.
[11] H.-G. Jung, S.-T. Myung, C.S. Yoon, S.-B. Son, K.H. Oh, K. Amine, B. Scrosati, Y.-K. Sun, Energy Environ. Sci. 4 (2011) 1345–1351.
[12] S.C. Lee, S.M. Lee, J.W. Lee, J.B. Lee, S.M. Lee, S.S. Han, H.C. Lee, H.J. Kim, J. Phys. Chem. C 113 (2009) 18420.
[13] Y. Wang, H. Liu, K. Wang, H. Eiji, Y.R. Wang, H. Zhou, J. Mater. Chem. 19 (2009) 6789.
[14] T.-F. Yi, J. Shu, Y.-R. Zhu, X.-D. Zhu, C.-B. Yue, A.-N. Zhou, R.-S. Zhu, Electrochim. Acta 54 (2009) 7464.
[15] S. Bach, J.P. Pereira-Ramos, N. Baffier, J. Power Sources 81–82 (1999) 273.
[16] G.X. Wang, D.H. Bradhurst, S.X. Dou, H.K. Liu, J. Power Sources 83 (1999) 156.
[17] C.Y. Ouyang, Z.Y. Zhong, M.S. Lei, Electrochem. Commun. 9 (2007) 1107–1112.
[18] Z. Zhong, C. Ouyang, S. Shi, M. Lei, Chem. Phys. Chem. 9 (2008) 2104–2108.
[19] D. Liu, C. Ouyang, J. Shu, J. Jiang, Z. Wang, L. Chen, Phys. Status Solidi (b) 243 (2006) 1835.
[20] P. Hohenberg, W. Kohn, Phys. Rev. 136 (1964) B864.
[21] M.D. Segall, P.J.D. Lindan, M.J. Probert, C.J. Pickard, P.J. Hasnip, S.J. Clark, M.C. Payne, J. Phys.: Condens. Mat. 14 (2002) 2717.
[22] J.P. Perdew, S. Burke, M. Ernzerhof, Phys. Rev. Lett. 77 (1996) 3865.
[23] Z. Wu, R. Cohen, Phys. Rev. B 73 (2006) 235116.
[24] J.P. Perdew, J.A. Chevary, S.H. Vosko, K.A. Jackson, M.R. Pederson, D.J. Singh, C. Fiolhais, Phys. Rev. B 46 (1992) 6671.
[25] B. Hammer, L.B. Hansen, J.K. Norskov, Phys. Rev. B 59 (1999) 7413–7421.
[26] S.H. Vosko, L. Wilk, M. Nusair, Can. J. Phys. 58 (1980) 2100.
[27] D.M. Ceperley, B.J. Alder, Phys. Rev. Lett. 45 (1980) 566.
[28] L. Aldon, P. Kubiak, M. Womes, J.C. Jumas, J. Olivier-Fourcade, J.L. Tirado, J.I. Corredor, C. Pérez Vicente, Chem. Mater. 16 (2004) 5721.
[29] C.M. Julien, K. Zaghib, Electrochim. Acta 50 (2004) 411.
[30] R. Baddour-Hadjean, J.-P. Pereira-Ramos, Chem. Rev. 110 (2010) 1278.
[31] T.-F. Yi, Y. Xie, J. Shu, Z. Wang, C.-B. Yue, R.-S. Zhu, H.-B. Qiao, J. Electrochem. Soc. 158 (2011) A266–A274.
[32] P. Kichambare, N. Kijima, H. Honma, S. Ebisu, S. Nagata, J. Phys. Chem. Solids 57 (1996) 1615–1620.
[33] J. Shu, J. Solid State Electrochem. 13 (2009) 1535.
[34] S. Panero, P. Reale, F. Ronci, B. Scrosati, P. Perfetti, V. Rossi Albertini, Phys. Chem. Chem. Phys. 3 (2001) 845–847.
[35] L. Shen, C. Yuan, H. Luo, X. Zhang, K. Xu, Y. Xia, J. Mater. Chem. 20 (2010) 6998–7004.
[36] M. Aydinol, A. Kohan, G. Ceder, Phys. Rev. B 56 (1997) 1354.
[37] J.D. Cox, D.D. Wagman, V.A. Medvedev, CODATA Key Values for Thermodynamics, Hemisphere Publishing Corp., New York, 1984, 1 pp.
[38] W.-s. Qiu, Y.-j. Li, Z.-w. Zhao, G.-s. Huo, X.-m. Xi, P.-p. Chen, Chin. J. Nonferrous Metals 20 (2010) 2260–2268.
[39] J. Shu, T.-F. Yi, M. Shui, Y. Wang, R.-S. Zhu, X.-F. Chu, F. Huang, D. Xu, L. Hou, Comput. Mater. Sci. 50 (2010) 776–779.
[40] I. Belharouak, Y.-K. Sun, W. Lu, K. Aminea, J. Electrochem. Soc. 154 (2007) A1083.
[41] B. Tian, H. Xiang, L. Zhang, H. Wang, J. Solid State Electrochem. 16 (2012) 205–211.
[42] T.-F. Yi, Y. Xie, Y.-R. Zhu, J. Shu, A.-N. Zhou, H.-B. Qiao, J. Power Sources 198 (2012) 318–321.
[43] J.W. Jiang, J.R. Dahn, Electrochim. Acta 49 (2004) 4599.
[44] D.D. MacNeil, J.R. Dahn, J. Electrochem. Soc. 149 (2002) A912.
[45] J. Yamaki, H. Takatsuji, T. Kawamura, M. Egashira, Solid State Ionics 148 (2002) 241.
[46] H.H. Lee, C.C. Wan, Y.Y. Wang, J. Electrochem. Soc. 151 (2004) A542.
[47] Q.S. Wang, J.H. Sun, X.L. Yao, C.H. Chen, J. Electrochem. Soc. 153 (2006) A329.
[48] E.P. Roth, D.H. Doughty, J. Franklin, J. Power Sources 134 (2004) 222.
[49] D. Aurbach, Y. Ein-Eli, O. Chusid, Y. Carmeli, M. Babai, H. Yamin, J. Electrochem. Soc. 141 (1994) 603–611.
[50] D. Aurbach, B. Markovsky, A. Shechter, Y. Ein-Eli, H. Cohen, J. Electrochem. Soc. 143 (1996) 3809–3820.
[51] O. Chusid, E. Ein Ely, D. Aurbach, M. Babai, Y. Carmeli, J. Power Sources 43 (1993) 47–64.
[52] J.W. Jiang, J.R. Dahn, Electrochem. Solid-State Lett. 6 (2003) A180.